Supporting Information

Microchannels with Self-Pumping Walls

Tingting Yu,[†,‡] Athanasios G. Athanassiadis,[*,†] Mihail N. Popescu,[†] Vijayakumar Chikkadi,[†,§] Achim Güth,[¶] Dhruv P. Singh,[†,‖] Tian Qiu,[*,†,‡] and Peer Fischer[†,‡]

†*Max Planck Institute for Intelligent Systems, Heisenbergstr. 3, 70569 Stuttgart, Germany*

‡*Institute of Physical Chemistry, University of Stuttgart, Pfaffenwaldring 55, 70569 Stuttgart, Germany*

¶*Max Planck Institute for Solid State Research, Heisenbergstr. 1, 70569 Stuttgart, Germany*

§*Current address: Department of Physics, Indian Institute of Science Education and Research, Dr Homi Bhabha Rd, 411008 Pune, India*

‖*Current address: Department of Physics, Indian Institute of Technology Bhilai, 492015 Raipur, India*

E-mail: thanasi@is.mpg.de; tian.qiu@ipc.uni-stuttgart.de

Supplementary Note 1

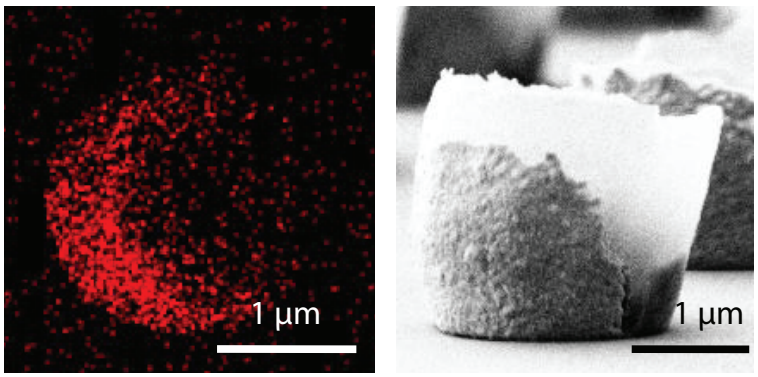

Figure S1: EDX (top view) and SEM image of a TiO2/Au micro pillar. Red represents Au.

Supplementary Note 2

The calibration of the diffraction pattern using the defocusing method with a phase contrast microscope is conducted by immersing and immobilizing 1 µm PS spheres in a 3 % polyacrylamide (PAC) gel.[1] The reference stacks are shown in Figure S2a, and the corresponding diffraction pattern area vs. defocusing height is plotted in Figure S2c. The flow profile is measured by focusing at different z positions in the channel. The error in the value of the height z, after accounting for the accuracy of the measurement system and the polydispersity of the PS spheres (variations in size of $\pm$ 0.1 µm from the nominal 1 µm), is approximately $\pm$2 µm.

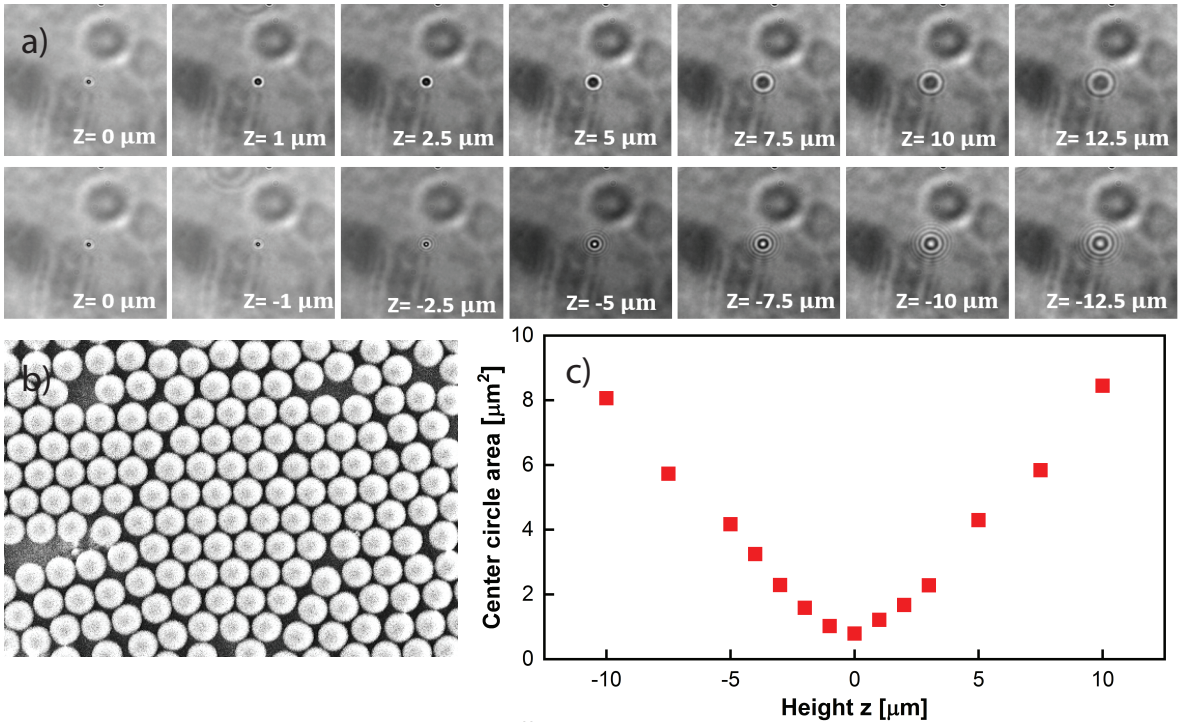

Figure S2: (a) Reference stacks of 1 µm PS spheres imaged at different distances z from the focal plane. (b) SEM image of 1 µm PS spheres used for fluid tracking. (c) Relationship between the calculated diffraction pattern area and the distance (height) from the focal plane.

Supplementary Note 3. Fabrication of various topographical structures and comparison of pumping speeds

The fabrication of 3D Janus bars and 2D patches is achieved using photolithography and Glancing Angle Deposition. The 3D bars are fabricated similar to the 3D pillars described in the main text. The only difference is the photomask, which is patterned with micro rectangular structures to produce the bars. For 2D Janus patches, an array of micro holes with thickness of 1.7 µm was exposed at 0° to an e-beam source with Au in a GLAD chamber for a 100 nm thick deposition, at 30° to TiO_2 for a 50 nm thick deposition, followed by a lift-off process in acetone and air plasma and an annealing process at 450°C for 2h in air. The SEM images of the corresponding structures are shown in Figure S3a and Figure S3b, respectively.

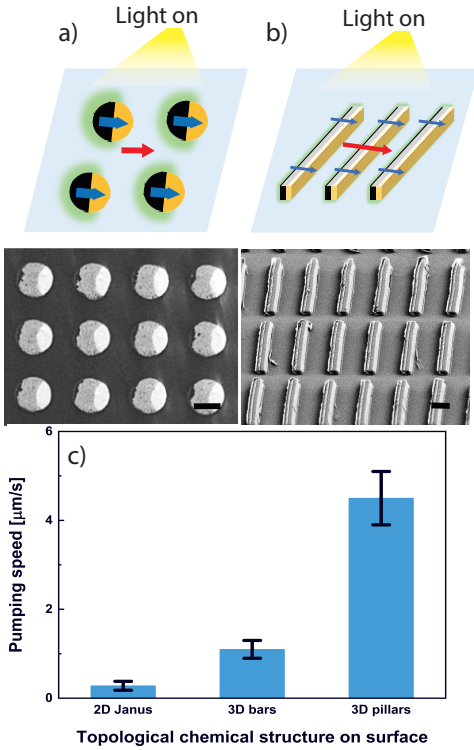

Figure S3: (a,b) Schematic (top) and SEM images (bottom) of a surface topologically patterned with (a) 2D Janus disk and (b) 3D Janus bar structures, respectively; the scale bars correspond to 1.5 µm. (c) Comparison of pumping behavior between different surface structures.

Supplementary Note 4. Analytical model of flow profile control

To model the fluid behavior, we consider a 2D flow in a thin channel, with overall length L much larger than the channel height h. Because of how the channels are fabricated, only a central portion of the channel contains the active surface. Therefore, we model the channel as consisting of three sections: an inert inlet of length L_1 (region 1), an active central region with length L_0 (region 0), and an inert outlet with length L_1 (region 2). All three regions have the same height h. A schematic of the channel geometry is shown in Fig. S4.

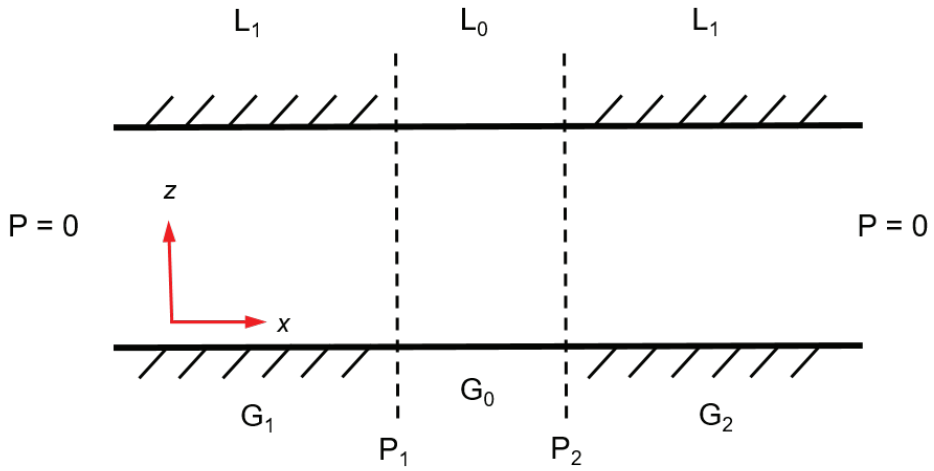

Figure S4: Illustration of the analytical model and parameters of a cross section of a channel. The sections L_1 are assumed to be passive (bare surfaces). The section containing pillars is indicated as L_0. P_1 and P_2 are the pressure at the inlet and outlet of the active section. See text for details.

We assume that the inlet and outlet pressures are at a constant hydrostatic pressure, defined as $P = 0$. Because the active region is the sole source of fluid motion, it must generate a pressure gradient to drive the flow. Therefore, we define P_1 and P_2 as the pressures at the start and end of the active region.

The fluid flow within each region of the channel is described by the continuity equation $\nabla \cdot (\rho \mathbf{u}) = 0$ and the Navier-Stokes equations. For an incompressible fluid in a thin channel

$h \ll L$, the fluid flows only along the channel, so that only the x-component of the velocity (u) is nonzero. In this case, the continuity equation is reduced to $\partial u/\partial x = 0$, indicating that the flow profile is a constant along the propagation direction. Further assuming that the flow is steady ($\partial u/\partial t = 0$) and that gravity is negligible within the channel, the Navier-Stokes equations reduce to the well-known form for Stokes flow in a 2D channel:[2]

$$\frac{dp}{dx} = \mu \frac{d^2u}{dz^2}, \tag{1}$$

Here $p(x)$ is the (z-independent) pressure in the channel the channel, μ is the fluid viscosity, and $u(z)$ is the fluid velocity in the x-direction.

Because the pressure depends only on x and the velocity only on z, the pressure must change linearly with x in each region of the channel. For convenience, we define the constant pressure gradient as $dp/dx = -G$. Then we can write the pressure gradient G across each section of channel as:

$$G_0 = \frac{P_1 - P_2}{L_0} \tag{2}$$

$$G_1 = -\frac{P_1}{L_1} \tag{3}$$

$$G_2 = \frac{P_2}{L_1}, \tag{4}$$

The flow profile $u(z)$ is solved by integrating Eq. (1) and applying boundary conditions at $z = 0$ and $z = h$. For wall velocities at the bottom and top of the channels of $u(z = 0) = u_w^b$ and $u(z = h) = u_w^t$, respectively, the solution to Eq. (1) is:

$$u(z) = -\frac{G}{2\mu}\left(z^2 - zh\right) + (u_w^t - u_w^b)\frac{z}{h} + u_w^b. \tag{5}$$

To completely determine the flow profile in the 3-part channel, the unknown pressures P_1 and P_2 (and thus G_1, G_2, and G_0) must be specified in terms of the (controllable) wall slip velocities, u_w^t and u_w^b, within the active region. To relate these quantities, we leverage

the incompressibility of the water, observing that the volume flow rate must be constant through all three sections of the channel. The volumetric flow rate (per unit depth of the channel into the page), $\dot{Q}$, is calculated in each section (indexed here by i) by integrating the flow speed over the whole channel height:

$$\dot{Q}_i = \int_0^h u_i(z)dz. \tag{6}$$

Enforcing continuity, $\dot{Q}_1 = \dot{Q}_2 = \dot{Q}_3 \equiv \dot{Q}$, will provide the necessary constraints to completely determine the unknown pressures P_1 and P_2, thereby fully describing the flow profile within the channel.

In the inert inlet and outlet segments, the flow profile will solve Eq. (1) with boundary conditions $u_w^b = u_w^t = 0$, so that

$$u_1(z) = -\frac{G_1}{2\mu}(z^2 - hz) \tag{7}$$

$$u_2(z) = -\frac{G_2}{2\mu}(z^2 - hz). \tag{8}$$

and the flow rates are

$$\dot{Q}_1 = \frac{1}{12}\frac{G_1}{\mu}h^3 \tag{9}$$

$$\dot{Q}_2 = \frac{1}{12}\frac{G_2}{\mu}h^3. \tag{10}$$

Enforcing $\dot{Q}_1 = \dot{Q}_2$ leads to the condition

$$P_1 = -P_2. \tag{11}$$

Assuming the flow is from left to right, $P_2 > 0$. The pressure head generated by the active walls is $\Delta P = 2P_2$, and the pressure gradient within the active region is $G_0 = -2P_2/L_0$.

Within the active region, the flow rate is

$$\dot{Q}_0 = \frac{G_0}{12\mu}h^3 + \frac{1}{2}\left(u_w^t + u_w^b\right)h \tag{12}$$

$$= -\frac{P_2}{6\mu L_0}h^3 + \frac{1}{2}\left(u_w^t + u_w^b\right)h. \tag{13}$$

Equating Eq. (13) with Eq. (9), the pumping pressure P_2 can be expressed in terms of the wall velocities and the channel geometry:

$$P_2 = \frac{6\mu}{h^2}\frac{L_1 L_0}{L_0 + 2L_1}\left(u_w^t + u_w^b\right). \tag{14}$$

Finally, the flow velocity and flow rate can be rewritten in terms of the wall velocities and channel geometry:

$$u(z) = \frac{6L_1}{L_0 + 2L_1}\left(u_w^t + u_w^b\right)\left(\frac{z^2}{h^2} - \frac{z}{h}\right) + \left(u_w^t - u_w^b\right)\frac{z}{h} + u_w^b \tag{15}$$

$$\dot{Q} = \frac{1}{2}\frac{L_0}{L_0 + 2L_1}\left(u_w^t + u_w^b\right)h \tag{16}$$

For each of the three channel configurations considered in the text (symmetric, antisymmetric, and skew), we now substitute the appropriate channel geometry and boundary conditions to calculate the flow profile, net flow rates, and pumping pressure using Eqs. (14)-(16).

Symmetric channel: Active top and bottom surfaces

Aligning the structures on top and bottom surfaces to pump in the same direction, the active surface provides a forward slip velocity on both walls, $u_w^b = u_w^t = u_w$, so that

$$u_{symm}(z) = 12u_w\frac{L_1}{L_0 + 2L_1}\left(\frac{z^2}{h^2} - \frac{z}{h}\right) + u_w, \tag{17}$$

and the associated flow rate is:

$$\dot{Q} = u_w h \frac{L_0}{L_0 + 2L_1} \tag{18}$$

The pumping pressure is:

$$P_2 = \frac{12 u_w \mu}{h^2} \frac{L_1 L_0}{L_0 + 2L_1}. \tag{19}$$

When the active pumping region is much longer than the side channels ($L_0 \gg L_1$), $\dot{Q} = u_w h$, and all of the fluid is pumped forward in a plug flow ($u_1(z) = u_w$). By contrast, when the pumping region is much smaller than the side channels ($L_0 \ll L_1$), the flow rate is reduced by a factor $\frac{L_0}{2L_1}$: $\dot{Q} = u_w h L_0/(2L_1)$. By adding longer inlets and outlets, flow resistance increases and the flow rate for a given slip velocity decreases.

Antisymmetric channel: Active top and bottom surfaces

When the active walls are assembled to pump in opposite directions, $u_w^b = u_w$ and $u_w^t = -u_w$. Applying the boundary conditions, the flow within the active channel follows a linear profile:

$$u_{asymm}(z) = u_w \left(1 - 2\frac{z}{h}\right). \tag{20}$$

Because of the odd symmetry of this configuration, the antisymmetric channel generates no unidirectional pumping pressure and no net flow:

$$P_2 = 0 \tag{21}$$

$$\dot{Q} = 0 \tag{22}$$

Skew channel: Active bottom surface

When only the bottom surface in a channel is active, $u_w^b = u_w$ and $u_w^t = 0$, and the flow profile within the active region is then a skew parabola:

$$u_{skew}(z) = 6u_w \frac{L_1}{L_0 + 2L_1} \left(\frac{z^2}{h^2} - \frac{z}{h} \right) + u_w \left(1 - \frac{z}{h} \right), \tag{23}$$

and the associated flow rate is

$$\dot{Q} = \frac{u_w h}{2} \frac{L_0}{L_0 + 2L_1}. \tag{24}$$

The pumping pressure is

$$P_2 = \frac{6u_w \mu}{h^2} \frac{L_0 L_1}{L_0 + 2L_1} \tag{25}$$

By comparing to Eqs. (19) and (18), we see that when pumping with only one active wall, the generated pressure and flow rate are half of those generated by the channel with two active walls.

Additional comments

By assuming that the flow u is independent of position along the channel x, the analysis above inherently ignores inlet/outlet effects, including at the boundary between the active and inactive regions. Because of the sudden change from slip- to nonslip- boundary conditions, an additional pressure drop is expected to occur locally, and u will become dependent on x. As a result, there must be some flow also in the z- direction locally around the boundary. However, these effects will remain localized to the interface between regions, and can be neglected to leading order as long as the channel regions are much longer than they are wide. In this case, the core implications of the model above remain valid: the flow profile described by Eq. 5 develops in each section, the magnitude of the pumping pressure can be estimated from mass conservation, and the volumetric flow rate is accurately calculated from mass conservation.

The validity of the model is supported *a posteriori* from the agreement with experimental data in Fig. 5 (main text) and from the results of a numerical simulations described below.

Supplementary Note 5. Numerical simulation

Numerical studies were conducted using COMSOL 5.3 with creeping flow physics to cross-check the validity of the approximations in the analytical model above. The simulation setup consists of 3 main sections of the channel (inactive-active-inactive) as shown in .png S5. The specific lengths L_1 and L_0 used for the numerical solution are those corresponding to the patterned surfaces and illumination area as used in the experiments (see Table 1 below). The inlet and outlet pressures are $P = 0$ Pa. At inactive walls, non-slip boundary conditions are enforced. At each active wall, the prescribed slip velocity is applied. The value of this velocity is taken from experimental measurements, as described in Note 6.

To avoid a discontinuity in the wall slip speed, small transition sections are added between each inactive and active section. The length of the transition sections are 0.5 µm with a ramping velocity along each active wall 0 µm/s to u_w (at the entrance to the active region) or u_w to 0 µm/s (at the exit). Given that the numerical and analytical solutions agree, we find that these transition sections do not significantly affect the results.

S5 shows the flow profiles for the three configurations of interest: skewed (1-wall) pumping, parallel (2-wall) pumping, and antiparallel (2-wall) pumping.

In Figure 5 of the main text, the x-velocity at $x = 0$ is plotted as a function of height in the channel z. It matches the analytical solution and agrees well with the experimental results.

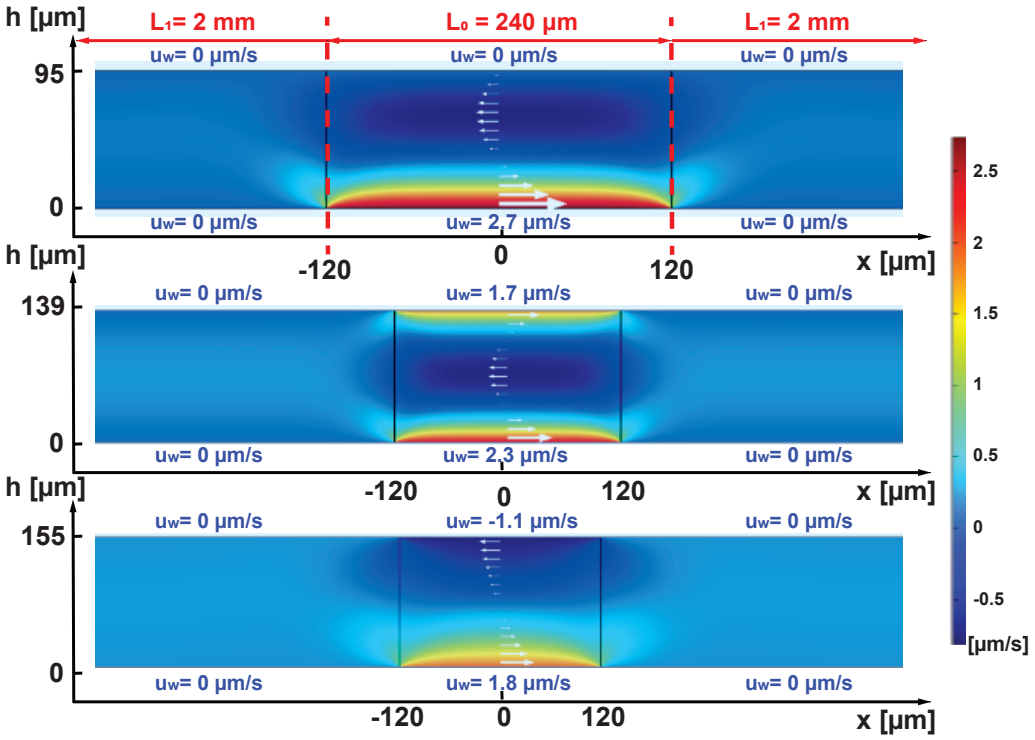

Figure S5: COMSOL results for the hydrodynamic flow within active channels with (a) bottom surface active pumping (b) top and bottom surface active pumping in same direction (c) top and bottom surface active pumping in opposite directions.

Supplementary Note 6. Parameters used in theoretical and numerical calculations

As shown in Figure 3b of the main text, tracer particles close to the active surface undergo a zigzag motion due to the hydrodynamic influence of the pillars. Therefore, flow velocity measurements along the channel are underestimated when tracking such particles. For the analytical and numerical analysis of flow within the active channels (in Figure 4), we do not consider the speed measured directly at the wall, and instead use particle velocities measured at least 5 µm from the wall. To account for this difference from the experiments we model the channel with a smaller height, corresponding to the distance between the uppermost and lowermost measured particle velocities. We then treat these velocities as the slip condition within the channel. The channel sizes and wall velocities used in the models for Fig. 5 are listed in Table 1.

Table 1: Parameters used in theoretical and numerical calculation

			symmetric	anti-symmetric	skew
Active Region Length	L_0	[µm]	240	240	240
Inactive Region Length	L_1	[µm]	2000	2000	2000
Experimental Channel Height	h_{exp}	[µm]	170	170	110
Modeled Channel Height	h	[µm]	139	155	95
Top-wall velocity	u_w^t	[µm/s]	1.74	-1.07	0
Bottom-wall velocity	u_w^b	[µm/s]	2.32	1.81	2.74

References

1. Taute, K. M.; Gude, S.; Tans, S. J.; Shimizu, T. S. High-Throughput 3D Tracking of Bacteria on a Standard Phase Contrast Microscope. *Nat. Commun.* **2015**, *6*, 1–9.

2. Acheson, D. J. *Elementary Fluid Dynamics*; Oxford Applied Mathematics and Computing Science Series; Clarendon Press ; Oxford University Press: Oxford : New York, 1990.